Graphene and Graphene Oxide (Raman Spectroscopy)

Graphene and Graphene Oxide (Raman Spectroscopy)

Amelia Carolina Sparavigna

Department of Applied Science and Technology, Polytechnic University of Turin, Italy

Email: amelia.sparavigna@polito.it

In previous discussions we have considered the Raman spectra of specific carbon-based materials, such as diamond, graphite, and the biochar resulting from pyrolysis of biomass. We have shown how the spectra can be decomposed, according to the intended number of components and the considered line shapes. Here, we approach the Raman spectra of graphene and graphene oxide, to understand how many components are required to interpret the related fingerprints.

Keywords: Raman spectroscopy, Spectrum decomposition, q-Gaussian Tsallis lines, Graphene, Graphene oxide, Carbon-based materials.

Introduction

The modern Raman spectroscopy is based on the photons scattered by a sample when a laser light shines on it. In the inelastic scattering processes, the emitted photons have a frequency shift, the Raman shift, which is producing the "fingerprint" typical of the investigated material. To the best of my knowledge, the first use of the term "fingerprint" for Raman spectroscopy was in the article by Fenske et al., 1947, about the Raman spectra of hydrocarbons. From that time on, the points of identification, such as the positions of peaks, shoulders and valleys have been considered to constitute the characteristic spectral pattern, that is, the "fingerprint" of a given material. For the carbon-based materials, the Raman spectroscopy is "a particularly well-suited technique" (Zhang et al., 2022), due to the "*long-range* crystalline vibrations and *short-range* molecular vibrations of carbon species", which are producing, for the different materials, their characteristic spectral fingerprints. According to Zhang and coworkers, these fingerprints allow identifying the "specific carbon materials including graphite, diamond, graphene, carbon nanotubes, fullerene, and amorphous carbon". To these materials, we must also add the recent studies on "graphene, bilayer graphene, and two-dimensional graphene heterostructures" (Zhang et al., 2022, Mu and Sun, 2020, Cui and Sun, 2021).

We have already discussed diamond and graphite Raman spectra in the framework of their decomposition in q-Gaussian Tsallis functions. Diamond has a Raman peak at 1332 cm^{-1}, corresponding to the vibration of its two Bravais lattices of carbon atoms with respect to each other (Krishnan, 1945). The crystalline graphite has a G peak at 1582 cm^{-1} and a G' (or 2D) peak at 2700 cm^{-1} (Malard et al., 2009). In other carbonaceous materials, such as soot, kerogen, and biochar, besides the G band we find the D1, D2, D3 and D4 bands mentioned by Beyssac et al., 2002, and Sadezky et al., 2005. In Claramunt et al., 2015, we can find a different notation where D is D1, D2 is D', D3 is D'' and D4 is D*. In Sousa et al., 2020, a further D5 component is used (see for instance the Raman spectrum decomposition in their Figure 2). Sadezky and coworkers give the following Raman shifts (cm^{-1}): ~1580 (G), ~1350 (D1), ~1620 (D2), ~1500 (D3), ~1200 (D4). Let us add ~1700 (D5), according to Sousa et al., 2020.

Here, our aim is that of showing spectra of graphene and graphene oxide, with respect to the graphite spectrum, to understand how many components are required to interpret the fingerprints. Graphene is a two-dimensional honeycomb lattice of carbon atoms that is widely considered for theoretical and applies studies, and for its technological potentials. Raman spectroscopy is considered suitable to characterize it and its related materials (Childres et al., 2013). "A large amount of information such as disorder, edge and grain boundaries, thickness, doping, strain and thermal conductivity of graphene" can be obtained from the spectrum recorded under different physical conditions, as discussed by Childres and coworkers. It means that Raman fingerprints must be able to give

the proper information, when decomposed in a convenient manner.

Comparing graphene, defective graphene and graphite spectra

In Ott and Ferrari, 2024, we can find a concise overview of light scattering processes, especially of the Raman scattering process in graphene. We can see how the Raman peaks are generated by the presence of the optical phonons according to their dispersions in the Brillouin zone. We can also appreciate that the Raman spectrum is sensitive to the number of graphene layers, to the presence of defects and to the straining and doping of it. Therefore, we can find reiterated that the Raman technique "can give insight in the material's quality, the number of layers, and is sensitive to any changes in electric or magnetic fields, band structure and temperature, making it ideal to probe layered materials" (Ott and Ferrari, 2024).

The Fig.3 in Ott and Ferrari illustrates the modes and phonon dispersions for a single layer graphene, whereas in the Fig.4 we can see the Raman spectra of graphite, and pristine and defective graphene. The peaks in the spectra are described in the following manner. "The G peak 1580 cm^{-1} arises from an E_{2g} phonon stemming from the Γ-point, ... The D peak, corresponding to an A_{1g} phonon ..., is due to the breathing mode of six-atom rings and requires a defect for its activation (Ferrari and Robertson, 2000; Thomsen and Reich, 2000; Tuinstra and Koenig, 1970) to fulfill the fundamental Raman selection rule" (Ott and Ferrari, 2024). This peak is activated by a process involving a transverse optical (TO) phonon at the K point. Similarly, another resonance scattering process at K or K' produces the defect-activated D' peak. The combination D+D' is also present. Peaks 2D and 2D' are the second order modes of D and D', "where the momentum conservation is fulfilled by [the] scattering of two phonons with opposite wave vectors". Consequently, defects are not required for their activation and these peaks "are always present in the Raman spectrum of graphene" (Ott and Ferrari, 2024, Ferrari et al., 2006, Basko et al., 2009). Moreover, the G peak is the only peak in graphene Raman spectrum fulfilling "the fundamental Raman selection rule directly, as its origin is at the center of the Brillouin zone where q = 0" (Ott and Ferrari, 2024).

Looking at the Figure 4 by Ott and Ferrari we can see that graphite and pristine graphene have the same peaks with differences in intensity and presence of shoulders. Here in our Figure 1, we propose a sketch accordingly.

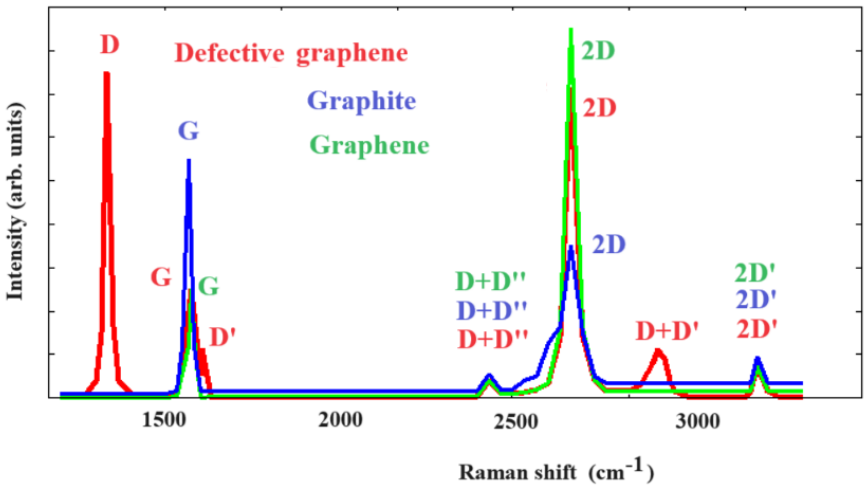

Fig. 1: A sketch of the Raman spectra of pristine Graphene (green), Defective graphene (red) and Graphite (blue) according to the spectra proposed in the Figure 4 by Ott and Ferrari, 2024. We can see that the peaks G, D+D'', 2D and 2D' are present in the three spectra. Peaks D, shoulder D' and peak D+D' are present in the defective graphene.

According to Childres et al., 2013, in graphene, "the Stokes phonon energy shift caused by laser excitation creates two main peaks in the Raman spectrum: G (1580 cm^{-1}), a primary in-plane vibrational mode, and 2D (2690 cm^{-1}), a second-order overtone of a different in plane vibration, D (1350 cm^{-1}) [Saito et al., 2011]. D and 2D peak positions are dispersive (dependent on the laser excitation energy) [Ferrari, A. C. (2007]." As stressed by Childres and coworkers, the given positions are for spectra excited by a 532 nm laser. Due to the presence of interactions between the layers of AB-stacked graphene, "as the number of graphene layers increases, the spectrum will change from that of single-layer graphene", and therefore we have a "splitting of the 2D peak into an increasing number of modes" (Childres et al., mentioning Ferrari et al., 2006). Moreover, the G peak is subjected to a small red shift according to the increased number of layers (Childres et al, 2013, Gupta et al., 2006). Consequently, in the case of AB-stacked graphene, the ratio of peak intensities, I_{2D}/I_G can be related to the number of layers, "as well as the position and shape of these peaks" (Childres et al., 2013, mentioning Ferrari et al., 2006).

The ratio I_D/I_G of the intensities of the D and G peaks is featuring the level of disorder in graphene. However, the increase of disorder in graphene is characterized by two regimes displayed by I_D/I_G. "There is a regime of "low" defect density, where I_D/I_G will increase as a higher defect density creates more elastic scattering" (Childres et al., 2013); however, we have also a "regime of "high" defect density, at which point I_D/I_G will begin to decrease as an increasing defect density results in a *more amorphous carbon structure, attenuating all Raman peaks* [as told by Lucchese, et al., 2010]"; Childres and coworkers, referring to Saito et al., 2011, consider these two regimes featuring "nanocrystalline graphite" and "mainly sp^2 amorphous carbon" phases, respectively. To characterize the disorder, we find also used the L_D length, that is, the average distance between defects, estimated by means of the Raman spectroscopy. In the Figure 3 by Childres and coworkers it is shown the Raman spectrum of graphene irradiated by electron beam, which is "showing significant D, D´ and D+G disorder peaks. The concentration of disorder can be extracted from the intensity ratio I_D/I_G".

For what is regarding the graphene edges, "a *strong D peak* will appear near armchair edges using an excitation laser *polarized* in a direction parallel to the line of the edge. This effect is significantly smaller for zigzag edges". It follows in the Childres and coworkers' article a discussion about the optical phonons active in armchair and zigzag edges. From the article, it seems that polarized Raman spectroscopy is relevant for graphene and related materials, and in fact we can find this spectroscopy mentioned by Wu et al., 2018, and Li et al., 2023.

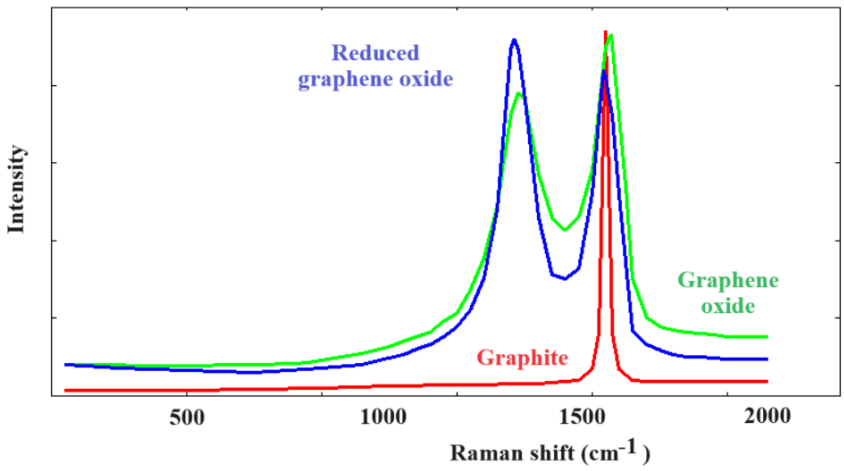

Fig.2: In Childres et al., 2013, we can find reproduced, in their Figure 5, the Raman spectra of graphite (red), graphene oxide (green) and reduced graphene oxide (blue), as given by Stankovich et al., 2007.

Introducing graphene oxide and reduced graphene oxide

In the Fig.5 by Childres et al., 2013, we can find reproduced the Raman spectra of SP-1 grade graphite, graphene oxide and reduced graphene oxide as given by Stankovich et al., 2007. So let us consider this reference. "Given [Stankovich and coworkers'] interest in the preparation of graphene-based materials …, [the researchers] set out to develop a general and reproducible approach for the preparation of graphene sheets from graphite. … [The researchers] decided to use graphite oxide (GO) as one possible route … [The proposed route] involved the complete exfoliation of GO into individual GO sheets followed by their in-situ reduction to produce individual graphene-like sheets [Stankovich et al., 2006]". The reduction of exfoliated GO sheets is made by using hydrazine. Stankovich and coworkers characterized the resulting material, presenting "evidence to support the claim that GO can be completely exfoliated into individual graphene oxide sheets and that chemical reduction of such sheets can furnish graphene-like sheets. GO is produced by the oxidative treatment of graphite via one of three principal methods developed by Brodie, 1860, Hummers and Offeman, 1958, and Staudenmeier, 1898, respectively" (Stankovich et al., 2007). According to Stankovich et al., 2007, and references therein, GO is made of oxidized graphene sheets. These sheets have the basal planes "decorated mostly with epoxide and hydroxyl groups, in addition to carbonyl and carboxyl groups located presumably at the edges (Lerf–Klinowski model)" (Stankovich et al., 2006). About this model, see for instance, the figure in Siklitskaya et al., 2021. The presence of oxygen functionalities is rendering the GO layers hydrophilic so that we can have water molecules "readily intercalate into the interlayer galleries. GO can therefore be also thought of as a *graphite-type intercalation compound* – as discussed by Stankovich and coworkers - with both covalently bound oxygen and non-covalently bound water between the carbon layers". A rapid heating of GO is producing delamination, because of the intercalated water evaporation and evolution of gases from pyrolysis (Stankovich et al., 2007, Schniepp et al., 2006). Being GO an electrical insulator, it cannot be used in his natural form for conductive nanomaterials. However, Stankovich and coworkers note that electrical conductivity of GO "can be restored close to the level of graphite by chemical reduction" (Stankovich et al., 2006, and references therein). Among the examined chemical reducing agents, hydrazine hydrate turned out to be the best, "in producing very thin graphene-like sheets".

About Raman peaks, Stankovich and coworkers note that the changes in the processing of pristine graphite into reduced GO are evidenced by the related Raman spectra. The researchers show the spectra that we sketched in our Figure 2. The given description is as follow: the pristine graphite spectrum has a prominent G peak at 1581 cm^{-1}, coming from the first-order scattering E_{2g} mode (Tuinstra and Koenig, 1970). The GO Raman spectrum has the G band *broadened and shifted* to 1594 cm^{-1}. The D band (1363 cm^{-1}) "becomes prominent, indicating the reduction in size of the in-plane sp^2 domains, possibly due to the extensive oxidation" (Stankovich et al., 2006). The rGO Raman spectrum has G and D bands, with peaks at 1584 and 1352 cm^{-1}, respectively., "with an increased D/G intensity ratio compared to that in GO. This change suggests a decrease in the average size of the sp^2 domains upon reduction of the exfoliated GO (Stankovich et al. mentioning Tuinstra and Koenig, 1970), and can be explained if *new graphitic domains* were created that are smaller in size to the ones present in GO before reduction, but more numerous in number" (Stankovich et al., 2007).

In the Introduction we have mentioned the work by Claramunt et al., 2015, which is regarding the Raman spectroscopy of GO and rGO (reduced graphene oxide). Claramunt and coworkers remember that Brodie, Staudenmaier, Hummers and Offeman proposed GO "as a carbon compound where oxygen functional groups are attached at carbon atoms within the hexagonal plane". Accordingly, "GO consists of two main regions constituted by hydrophobic π-conjugated C-sp^2 and the C-sp^3 domains. The latter are mainly constituted by alcohol and epoxy groups located at the basal plane and carboxylic acids groups at the structure edges" (Claramunt et al., 2015, mentioning Lerf et al., 1998). The control of oxygen functionalities attached to the carbo-layer is tuning the electronic and mechanical properties of GO, and therefore, GO "is often reduced by chemical agents, or thermal annealing, obtaining reduced graphene oxide (rGO)" (Claramunt et al., 2015, and references therein). For the reduction of GO, hydrazine or vitamin C are used. These agents introduce functional groups with amino nitrogen atoms when hydrazine is used or some O-groups with the reduction by means of vitamin C. "Alternatively, GO of different oxidation grade can be obtained by *thermal reduction*" (Claramunt et al., 2015, and reference there in).

According to Claramunt and coworkers, the chemical and thermal reductions are creating defects which alter "the physical and chemical properties of graphene-based materials. Then, taking into account the important role of defects in the properties of these materials, it becomes necessary to develop an *accurate methodology* to study them. Raman spectroscopy … has been widely used to study graphite and graphene" (Claramunt et al., mentioning Jorio et al., 2011). The researchers describe the spectra in the following manner. The Raman peaks in crystalline graphene are G (~1585 cm^{-1}) and 2D bands (~2700 cm^{-1}), that is first- and second-order Raman modes. The peaks change their width in the spectrum of GO. "These changes were attributed to high defect concentration related to the oxidation and are accompanied by the appearance of an intense peak centered at~1350 cm^{-1}, called the D band. The D band is related to the A_{1g} breathing mode, and it is observed because graphite oxidation and the subsequent reduction of GO seriously alter the basal plane structure of graphene" (Claramunt et al., 2015, and references therein). Other weak bands between 1100 and 1800 cm^{-1} can be observed in the spectra of GO as flakes and powders. These peaks are not present in pristine graphene or graphite. Some defects consist in "rings with different numbers of C atoms and configurations of C−O bonds. In these cases, a peak centered at~1620 cm^{-1}, D' band," is appearing (Claramunt et al., 2015, and references therein). Literature is also reporting a peak located between 1150 and 1200 cm^{-1} (D*) and a broad peak between 1500 and 1550 cm^{-1} (D'') (see the graphical abstract by Claramunt et al.). In soot and carbon black too, these peaks have been evidenced. Claramunt et al. provide an extensive and detailed discussion of literature about the origin of the peaks they mentioned.

Claramunt and coworkers are proposing several Raman spectra of GO and annealed GO. No significant differences are evidenced. "All the spectra present D and G peaks centered at~1350 cm^{-1} and~1585 cm^{-1} respectively, and the splitting of 2D Raman-active bands centered at ~2900 cm^{-1}. … an important feature is the presence of *a broad shoulder* between D and G peaks. The Raman spectral analysis of graphene derivatives often neglected this *shoulder* because it is very weak; nevertheless, it has been described in the Raman spectra of some carbon-based materials. Some authors fitted this shoulder using five functions which were ascribed to G, D, and D' bands and two poorly understood peaks, referred to as D*(~1150−1200 cm^{-1}) and D'' (~1500−1550 cm^{-1})" (Claramunt et al., and references therein). Claramunt and coworkers fitted the Raman spectra of GO and rGO with three pseudo-Voigt and two Gaussian functions. In their Figure 2b we can find an example for a Raman spectrum of rGO annealed at7 00°C. The sketch in our Figure 3 is showing this case. In the Figure 4a by Claramunt et al, we can find the dependence of the position of the D'' and D* bands with the oxygen content (and also in the graphical abstract of their work).

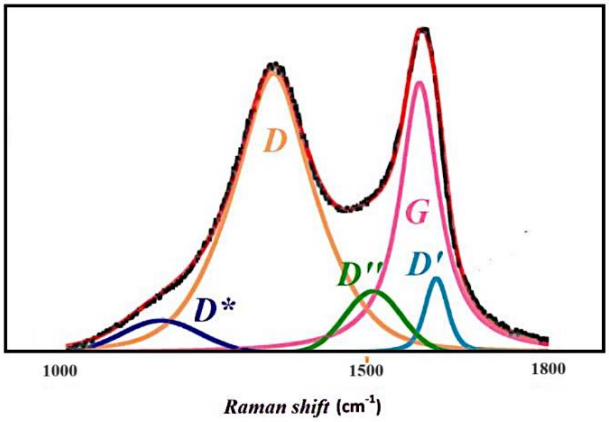

Fig. 3: A sketch of a Raman spectrum (first order part) in Claramunt et al., 2015, where we can find a notation of the peaks, different from that used by Beyssac et al., 2002, and Sadezky et al., 2005, where D is D1, D' is D2, D'' is D3 and D is D4.*

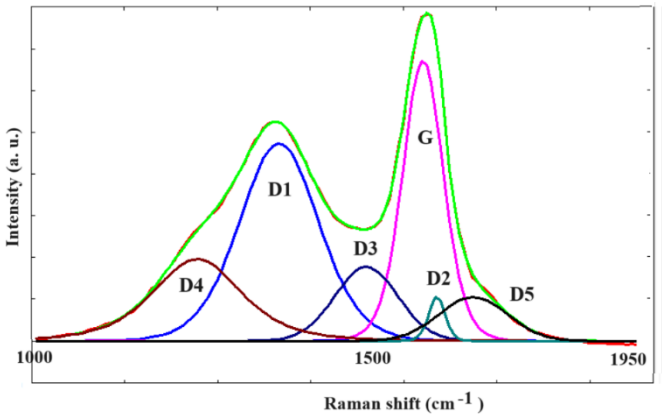

Fig. 4: Recovering the data (for biochar) from the Figure 2 by Sousa et al., 2020, we can propose a decomposition obtained by means of q-Gaussian Tsallis functions (see Appendix). From left to right, using Sousa et al. notation, the components are D4, D1, D3, G, D2 and D5. D5 is adjusting the fit (according to Sousa et al.).

For comparing the notations, in the Figure 4 we show the decomposition with q-Gaussian Tsallis functions (see Appendix) of the spectrum given by Sousa et al., 2020, in their Figure 2. In the shown decomposition, we used the q-Gaussians. These bell-shape functions are characterized by a shape parameter, the q—parameter, so that, when q is equal to 2 the curve is a Lorentzian curve. When q is close to 1, it is a Gaussian.

Graphene-based van der Waals (vdW) heterostructures

In Frisenda et al., 2020, graphite is mentioned among the naturally occurring van der Waals materials. It was "The exfoliation of two naturally occurring van der Waals minerals, graphite and molybdenite," that "shaped a whole new field of research", that of the 2D materials (Frisenda et al., 2020). In fact, in 2010, the Nobel Prize in Physics was awarded to Andre Geim and Konstantin Novoselov, for experiments regarding the two-dimensional graphene. The experiments concerned the exfoliation of graphite to obtain the single layers of graphene. Today, the "family of van der Waals materials that can be exfoliated to isolate 2D materials keeps growing" (Frisenda et al., 2020). Most materials are synthetic, but nature is providing plenty of van der Waals minerals that can have relevant applications. Therefore, it is fundamental to expand our investigation about Raman spectroscopy to van der Walls graphene-based heterostructures.

Let us consider Haidari et al., 2020, who studied the doping effect in graphene-graphene oxide interlayer. To study "the interlayer coupling effect in combined structures", Haidari and coworkers produced graphene and graphene oxide (GO) heterostructures. In particular, the researchers prepared graphene-, GO-, and graphene/GO areas on a SiO_2/Si substrate. The Raman spectra of these three regiones were then obtained. "As shown in Fig. 2a [in Haidari et al., 2020], the distinct Raman spectra for the three defined regions (graphene, GO, and graphene/GO) are clearly identified. For a CVD-fabricated monolayer graphene, the intensity ratio of 2D/G in the Raman spectra is determined to be approximately 3, which indicates that the graphene is crystalized".

The article by Haidari et al., 2020, is Open Access, under a Creative Commons Attribution 4.0 International License. Thanks to authors and Editor, we have the possibility to adapt the Figure 2 in Haidari et al., 2020, in our Figure 5.

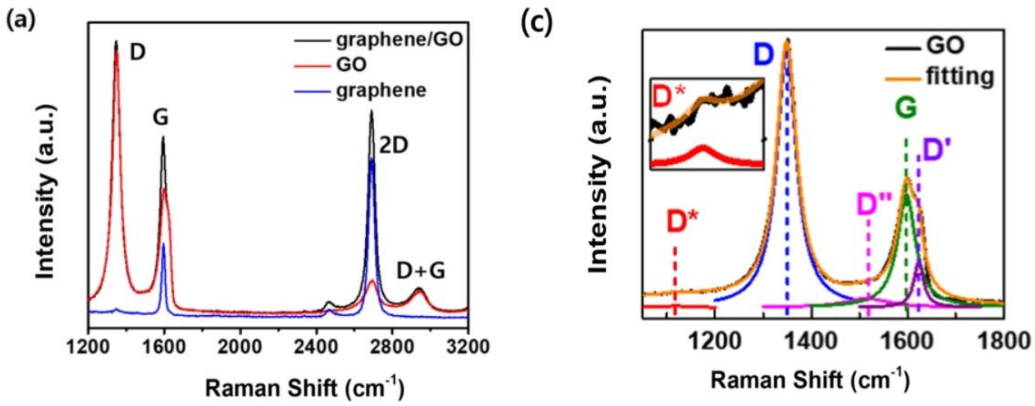

Fig. 5: Two panels of the Figure 2 in Haidari et al., 2020 (article and figures licensed under CC BY 4.0 DEED). The panel (a) is giving the Raman spectra, with evidenced the four peaks D, G, 2D, and D + G peaks, of graphene (blue), GO (red) and graphene/GO (black). For the D peak, the red and the black curves are almost coincident. Panel (c) is the Gaussian fitting results for the Raman spectrum of GO, with D (~1351 cm^{-1}), D' (~1623 cm^{-1}), D'' (~1515 cm^{-1}), G (~1597 cm^{-1}), and D (~1120 cm^{-1}) peaks.*

The simple building block

According to Li et al., 2023, "The fundamental mechanisms of Raman scattering of graphitic carbon materials have been revealed in detail thanks to the isolation and analysis of graphene, the simple building block of all graphitic carbon materials" (Li et al. are mentioning Novoselov et al., 2004, Ferrari et al., 2006, Geim and Novoselov, 2007). "Raman spectroscopy is particularly useful for the characterisation of graphene since its lack of a band gap means that all wavelengths of incident laser radiation are resonant" (Li et al. referring to Ferrari and Basko, 2013). This means that the Raman spectrum of graphene is massively resonantly enhanced enabling well-defined spectra to be obtained from graphene layers of only one atom in thickness" (referring to Ferrari et al., 2006). According to Li et al., the studies regarding graphene "have now solved many of the earlier unanswered questions for graphite and CNTs", carbon nanotubes. Li et al. are also concentrating on carbon fibers.

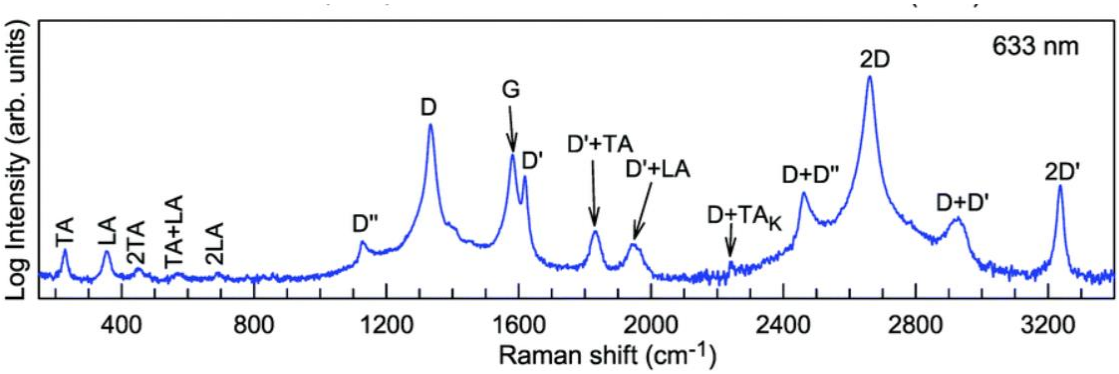

Fig. 6: The Raman modes in graphite whiskers (region from 150 to 3400 cm^{-1} excited at 632.8 nm), as given by Wu et al., 2018, Open Access, under CC BY-NC 3.0 DEED License. Data are by Tan et al., 2001. Note please the details of the spectrum enhanced using the semi-logarithmic scale.

Li and coworkers show in their Figure 3(a), the "number of Raman bands and their overtones [that] can be observed for carbon materials", referring to Wu et al., 2018, stressing that "Care must therefore be exercised in the interpretation of Raman fingerprints of carbon materials as different structural features may give rise to a similar response". Let us consider Wu et al. and the Figure 3 of their article. The panel (a) in Li et al. is the panel (e) in Wu et al., which is giving "The expected Raman modes observed in graphite whiskers in the spectral region from 150 to 3400 cm^{-1} excited at 632.8 nm". The panel is told reproduced from Tan et al., 2001. Comparing the publications, it is evident that the figure 3(e) in the work by Wu et al. is an original layout, proposing data in a very detailed manner, and in semi-logarithmic scale (see our Figure 6). The article Wu et al., 2018, is Open Access, under CC BY-NC 3.0 DEED License. About graphite whiskers and other carbon-based materials, such as columnar carbons with a cone-shaped top, and needle- rods-like crystals, see Liu et al., 2023 Open Access.

From Wu et al., 2018, let us also propose their Figure 1, in the following Figure 7.

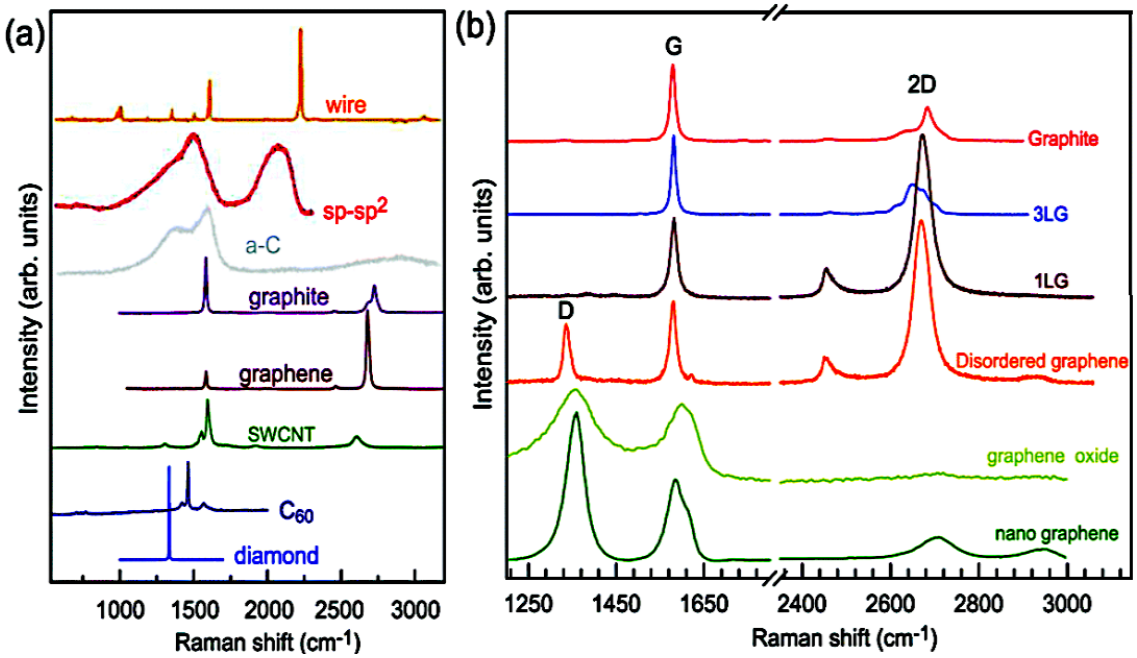

Fig. 7: The Figure 1 in Wu et al., 2018, CC BY-NC 3.0 DEED, is giving in the panel (a) the Raman spectra of "carbon solids and nanostructures, including 1D carbon wires, sp–sp^2 carbon, amorphous carbon (a-C), graphite, graphene, single-walled carbon nanotubes (SWNT), C60, and diamond. Raman spectra of carbon wire, sp–sp^2 carbon, a-C are reproduced with permission from" Milani et al., 2015, Open Access, CC BY 2.0 DEED, Copyright 2015, Beilstein-Institut. In the panel (b), we can see the Raman spectra of graphene-based materials, graphite, 1LG (monolayer graphene), 3LG, disordered graphene, graphene oxide and nanographene.

GO paper

Let us continue reading the article by Wu et al., 2018.

"Under suitable conditions, [see references in Wu et al.] GO can undergo complete exfoliation in water, yielding colloidal suspensions of almost entirely individual graphene oxide sheets. Such sheets can be chemically functionalized, dispersed in polymer matrices, and deoxygenated to yield novel composites" (Wu et al., referring to Stankovich et al., 2006). Among the novel composites we can find the Go paper. "GO sheets can be assembled into a paper-like material under a directional flow. Vacuum filtration of colloidal dispersions of graphene oxide sheets

yielded, after drying, free-standing GO papers with thicknesses ranging from 1 to 30 μm, as shown in Figure 31(a)" (Wu et al., referring to Dikin et al., 2007, and regarding the preparation and characterization of graphene oxide paper). In the panel (b), as evidenced by Dikin et al., we have well-packed layers through the cross-section of the GO paper. The Fig. 31(d) contains the Raman spectra of a typical GO paper. "The G peak and 2D peak are characteristic of sp^2 hybridized carbon–carbon bonds in graphene. The strong and broad D band and high I(D)/I(G) ratio in GO confirm its lattice distortions and a large amount of sp^3-like defects caused by the oxidation process" (Wu et al., 2018).

The article by Ejehi et al., 2020, Open Access, is proposing a use for the GO paper. In their research, a flexible graphene oxide (GO) paper was considered as the electrode for the Triboelectric Nanogenerators TENGs. "The all-flexible TENG has been employed as a self-powered humidity sensor to investigate the effect of raising humidity on the output voltage and current by applying mechanical agitation in two forms of using a tapping device and finger tapping". The article by Ejehi et al., 2020, is licensed under a Creative Commons Attribution 4.0 International License, http://creativecommons.org/licenses/by/4.0/. In our Figure 8, we reproduce the panels (c), (d) and (f) of the Figure 2 by Ejehi et al., 2020.

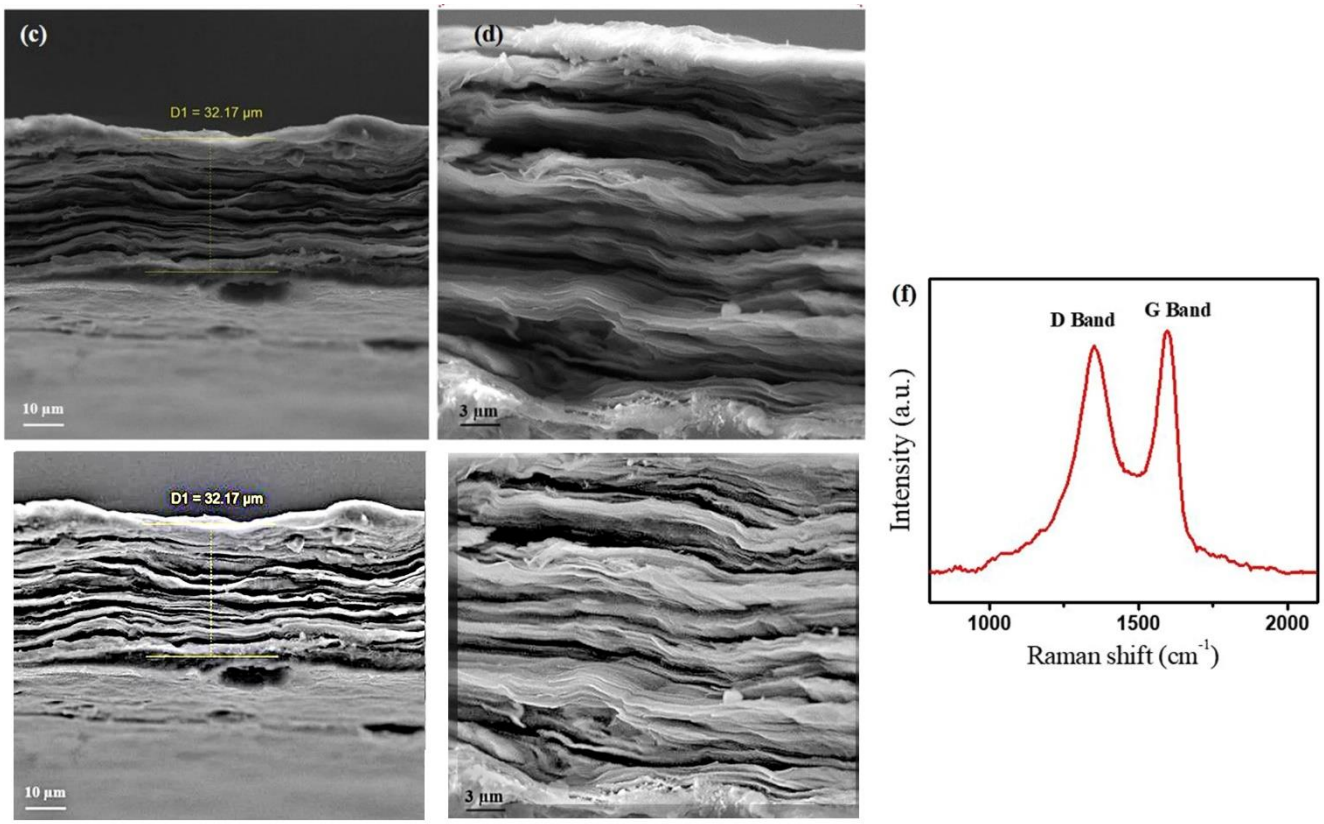

Fig. 8: In the upper part of the figure, we are showing the panels (c) and (d) in the Figure 2 by Ejehi et al., 2020, Open Access, CC BY 4.0 DEED. The panels show a cross section SEM image. In the panel (f) a Raman spectrum is given. Below the original panel (c) and (d), we are proposing an enhancement of the SEM images obtained by means of the GIMP Retinex tool.

A remark

Before continuing the discussion about the Raman spectrum of graphene oxide, let us consider the article by Goldie et al., 2020. “Raman data are usually acquired by using Raman microscopy which couples a Raman spectrometer to an optical microscope, allowing high-magnification visualization of a sample and Raman analysis with a microscopic laser spot. In common with other microscale techniques a single spectrum *should not be used to characterize a macroscopic material.* While it is common for a representative Raman spectrum of a carbon sample to be reported, this is undesirable because of the variations likely to be present” (Goldie et al., 2020).

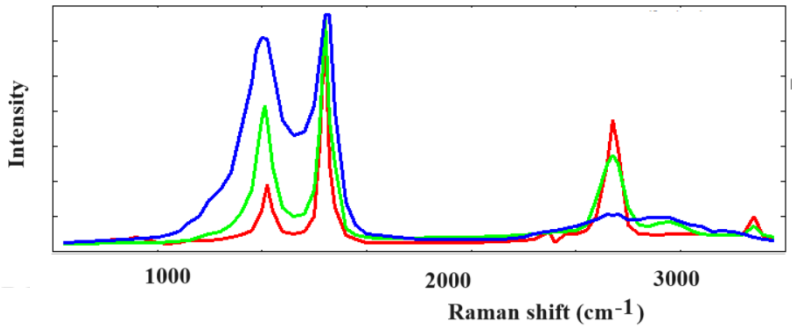

Fig.9: This sketch is representing what is given in the Fig.1a by Goldie et al., 2020. The three different spectra are coming from the same material.

Figure 1a, in Goldie et al., 2020, highlights what told by Goldie and coworkers, by means of *three different Raman spectra from the same material*. “Based on the evidence of only one spectrum, this material could be highly oxidized graphite or few-layer graphene, whereas in fact the sample is mostly graphitized carbon. One potential solution adopted by some is to collect multiple spectra from a sample and build a statistically meaningful picture of the material being analyzed” (Goldie et al., 2020). The spectra proposed in the Figure 1a by Goldie et al. is here given by the sketch in the Figure 9.

GO with different degrees of oxidation

In Sardinha et al., 2020, we can find the Raman spectra of GO with different degree of oxidation (see please the article for the detailed discussion of the preparation of GO). The researchers obtained five oxidation degrees with a synthesis which is using 2.0, 2.5, 3.0, 4.0, and 5.0 g of oxidizing agent for each 1.0 g of graphite. The authors are discussing the Raman spectroscopy of carbon-based materials, considering the features that we have already seen in the literature mentioned above. “The first order reveals the domain of two characteristic D and G bands.” The D band (from 1350 to 1380 cm^{-1}) is giving a measure of the disorder in the crystalline structure. The G band, from 1575 to 1600 cm^{-1}, “is a characteristic of carbon-carbon vibration in the plane of the aromatic layers” (Sardinha et al., 2020).

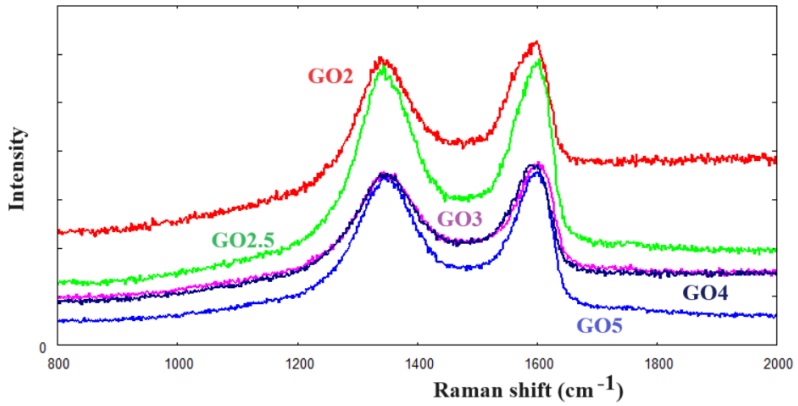

Fig.10: In Sardinha, 2019, Mendeley Data, CC BY 4 licensed, we can find the Raman spectra of GO with five different degrees of oxidation. The five oxidation degrees have been obtained with a synthesis using 2.0, 2.5, 3.0, 4.0, and 5.0 g of oxidizing agent for each 1.0 g of graphite. Here we show the first order part of the spectra.

The Fig.2 in Sardinha et al., 2020, is giving the spectra of graphite and GO with the five different oxidation degrees. The researchers conclude that the "GO spectra show G band with carbon domains with sp^2 hybridization and D band with carbon domains with sp^3 hybridization, which is also related to domains of O atoms. For second-order Raman spectra, [and Sardinha and coworkers mention Mishra and Ramaprabhu, 2012], four bands can be deconvoluted for GO spectrum with their respective peak positions of 2545 cm^{-1} (assigned to G*), 2690 cm^{-1} (assigned to 2D (G'')), 2925 cm^{-1} (assigned to D + D''), and 3160 cm^{-1} (assigned to 2D'')." (Sardinha et al., 2020). The comparison with graphite spectrum shows that "D band width increased as a function of the oxidation degree increase, which is associated with the increase of defects in the GO basal and edge planes." Moreover, Sardinha et al. mention the work by Ferrari and Robertson, that "attributed the [observed] G band displacement to the formation of new carbon atoms with sp^3 hybridization in the graphite network. They associated this displacement to the doping of the graphene layers or, in more oxidized samples, to the number of defects generated in the graphene sheets".

Following the literature about fitting processes, Sardinha et al. "established a method to fit GO Raman spectra with different oxidation degrees taking into account the disorder influence on first and second-order band features. Thus, the fitting for the first-order region was performed from 1000 to 1800 cm^{-1} using *five peaks* named as D*, D, D**, G, and D'' at around 1190, 1350, 1500, 1580, and 1610 cm^{-1}". The researchers use a notation different from that of Claramunt et al. and from that of Sadezky et al., 2005. For what is regarding the I_D/I_G ratio, as "indicator of disorder degree", Sardinha and coworkers used the *peaks areas* and G as G_{app}= G + D'', referring to King et al., 2016. A very interesting result is given for the A_D/A_{Gapp} behavior in Fig. 4 by Sardinha et al., 2020.

In King et al., 2016, it is remarked that "the peak commonly labelled G in the Raman spectra of GO and rGO samples is in fact a *superposition* of the G and D' peaks (the G_{app} peak) [in the Claramunt et al. notation]" (see examples in the Figure 2 by King et al.). The apparent G peak is named as "G_{app}". "This superposition renders the I_D/I_{Gapp} ratio an unreliable measure for the reduction of GO and has prevented it from accurately describing some of the recently reported GO and rGO samples. [King et al.] propose that the best measure of GO reduction is the difference in the positions of the D'_{inf} and G_{app} peaks, i.e. $D'_{inf} - G_{app}$" (King et al., 2016). The inferred D' mode is named as "D'_{inf}".

Interpretation (Ferrari and Robertson)

Sardinha and coworkers are referring, among many others, to the work by Ferrari and Robertson, 2000. Let us consider this article because of the interpretation we can find in it of D and G bands. As told by Ferrari and Robertson in their introduction, the "versatility of carbon materials" is due to their properties related to the ratio in them of sp^2-graphite-like to sp^3-diamond-like bonds. The sp^2-bonded carbons are producing a graphitic order, "ranging from *microcrystalline graphite to glassy carbon*". An amorphous carbon can be considered as a mixture of sp^3, sp^2, and

also sp^1 sites, with the presence of hydrogen up to 60%, resulting in compositions as in the ternary phase diagram shown in the Fig. 1 given by Ferrari and Robertson. In this diagram we can find the diamond-like carbon (DLC) defined as the amorphous carbon "with a significant fraction of sp^3 bonds" (for other materials, see please the discussion in Ferrari and Robertson).

The work by Ferrari and Robertson is centered on Raman spectroscopy. Diamond has the T_{2g} 1332 cm^{-1} zone center mode, according to Knight and White, 1989. The disordered graphite has two sharp peaks, G around 1580–1600 cm^{-1} and D around 1350 cm^{-1}, "usually assigned to zone center phonons of E_{2g} symmetry and K-point phonons of A_{1g} symmetry, respectively". And here, we find a fundamental observation made by Ferrari and Robertson: "The unusual fact is that G and D peaks, of varying intensity, position, and width, continue to dominate the Raman spectra of nanocrystalline and amorphous carbons, even those without widespread graphitic ordering".

Discussing the Raman processes in disordered carbons, according to Ferrari and Robertson, "the visible Raman spectrum depends fundamentally on the ordering of sp^2 sites and only indirectly on the fraction of sp^3 sites". The researchers continue presenting a "three-stage model relating the visible Raman parameters to the sp^2 nanostructure and content of disordered carbons". The Section III of their work is dedicated to the vibrational modes, and in its Figure 3 we can find the vibrational density of states, VDOS, of graphite (in fact, of a single layer graphene) and of diamond. "Graphite has a higher VDOS band limit than diamond because the sp^2 sites have stronger, slightly shorter bonds than sp^3 sites". Then, the VDOS of DLC is discussed, such as the related consequences on Raman spectra.

In the Section IV, we can find the "Raman scattering in disordered carbon". First, the "Raman modes in *single crystals* obey the fundamental selection rule $\mathbf{q}\approx 0$, where $\mathbf{q}$ is the wave vector of the scattered phonon". However, on phonons we have sample boundary effects and grain boundaries, that is, finite-size domains, and therefore "the selection rule is relaxed to allow the participation of phonons near Γ, with $\Delta q \sim 2\pi/d$, where d is the dimension of the crystalline domain". According to Nemanich, Solin, and Martin, 1981, "the Raman scattering intensity of a finite crystal is given by" (Eq.6 in Ferrari and Robertson):

$$I(\omega) = \frac{n(\omega)+1}{\omega}\sum_{q,j} C\left(q,\omega_j(q)\right)|F(q)|^2 \frac{\Gamma/2\,\pi}{\left(\omega-\omega(q)\right)^2+\Gamma^2/4}$$

where we have a weighted sum over phonon wave vectors and branches, of Lorentzian broadened phonon lines. Function $C\left(q,\omega_j(q)\right)$ is the Raman coupling coefficient, whereas $F(q)$ is a phonon wave-vector "uncertainty". The boson occupation factor is $n(\omega)$. In this equation, as shown by Nemanich and coworkers, we can find the dynamical structure factor for Stokes scattering, in origin the Fourier transform of the correlation function of fluctuations in the polarizability. The Lorentzian broadening, with a lifetime Γ for phonons, is substituting the δ function in the dynamical structure factor. In amorphous materials the intensity is given by the Shuker-Gammon formula, 1970:

$$I(\omega) = \frac{n(\omega)+1}{\omega} C(\omega) G(\omega)$$

Function $G(\omega)$ is the VDOS of the disordered network. This equation works well for *a*-Si and *a*-Ge, "which are sp^3 bonded only, … The visible Raman spectra of disordered carbons are in marked contrast" (Ferrari and Robertson, and references therein). "In contrast, the Raman spectra of all disordered carbons are dominated by the relatively sharp G and D features of the sp^2 sites. This could be ascribed to the much greater cross-section of the π states. Nevertheless, the prevalence of G and D-like features, even in amorphous carbons with little graphitic ordering, requires explanation" (Ferrari and Robertson, and references therein).

The G mode of graphite, E_{2g} symmetry, is a mode (see Fig.4 in Ferrari and Robertson) that "does not require the presence of sixfold rings, and so it occurs at all sp^2 sites, not only those in rings. It always lies in the range 1500–1630 cm^{-1}, as it does in aromatic and olefinic molecules" (Ferrari and Robertson, mentioning Lin-Vien et al., 1991). D peak, about 1355 cm^{-1}, is due to a breathing mode with A_{1g} symmetry, and the phonons which are involved are those close to the K zone boundary. "This mode is *forbidden in perfect graphite* and only becomes *active in the presence of disorder*. The D mode is dispersive; it varies with photon excitation energy, even when the G peak is not dispersive" (Ferrari and Robertson and references therein). Please, consider the further discussion in Ferrari and

Robertson about the D band and their "quasi selection rule".

In Ferrari and Robertson we find mentioned the work by Mapelli, 1998, Mapelli et al., 1999, who showed the main Raman features of aromatic oligomers as possessing the same symmetries, E_{2g} and A_{1g} , of graphite. "They also showed that the eigenvectors of these oligomers or clusters can be mapped onto those of graphite phonons along the direction GKM. In particular, … (see the discussion in Ferrari and Robertson) … This indicates that aromatic clusters can be considered as a part of a graphite superlattice, both electronically and vibrationally. This simultaneous mapping means that the behavior and dispersion of the D and G peaks in graphite also holds for aromatic oligomers and clusters in disordered carbon" (Ferrari and Robertson, 2000).

And here, let us show a remarkable Raman spectrum, that has been obtained by Gavilan et al., 2022, from the COSmIC pyrene-generated nanograins. COSmIC is the Cosmic Simulation Chamber facility at NASA Ames Research Center. Using Lorentzian and Gaussian components, Gavilan and coworkers determined six bands, and we can clearly see the G and the D (in particular, D1) bands.

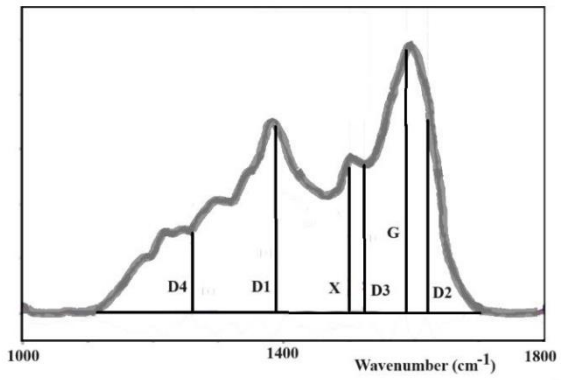

Fig.11: The grey line is giving the data obtained from COSmIC pyrene-generated nanograins, by Gavilan et al., 2022, in their Figure 5. Using Lorentzian and Gaussian components, Gavilan and coworkers determined six bands; the positions of their centers are here given by the black lines.

Let us return to Ferrari and Robertson, and to their point of view about the practical Raman spectroscopy.

"A practical point when *comparing different fitting parameters* for Raman spectra *is to know the fitting procedures used*. The Raman spectrum is a VDOS modified by a coupling coefficient, which incorporates various resonances. *There is no a priori reason to choose a particular function to fit the spectrum.* Empirically, the visible Raman spectra of amorphous carbons show one or two prominent features (the G and D peaks) and some minor modulations … The simplest fit consists of *two Lorentzians or two Gaussians*. A *Lorentzian fit is often used for crystals*, arising from *finite lifetime broadening*, and it is normally used for disordered graphite. A *Gaussian line shape* is expected for a *random distribution of phonon lifetimes in disordered materials*. A simple two symmetric-line fit is not always suitable, and one can find a multipeak fit" (Ferrari and Robertson, 2000).

"The most widely used alternative to a Gaussian fit is a Breit-Wigner-Fano (BWF) line for the G peak and a Lorentzian for the D peak". The BWF, which is asymmetric, can be reduced to a Lorentzian line shape for its specific feature parameter limit to 0. As observed by Ferrari and Robertson, the BWF curve has an increased power tail for lower frequencies. This allows the use of BWF lines to account for residual intensities, avoiding extra peaks. "The BWF+Lorentzian line pair is therefore an excellent means to fit Raman spectra of all carbons, from graphite to *ta*-C [tetrahedral amorphous carbon]. A Lorentzian line shape is used for the D peak as it is from the same family as the BWF line, while the various enhancement mechanisms for the D peak are consistent with a Lorentzian. However, any wide low-frequency tail of the BWF line will push the D peak to lower frequencies as the disorder increases. This significantly decreases the D peak size compared to a two-Gaussian fit. … . On one hand, smaller aromatic

clusters have higher modes and shift D upwards. … Another important issue … [of the BWF lineshape], is that the maximum of the BWF line is not at ω_0 but lies at lower frequencies … [However] The asymmetric BWF line shape is appropriate for the G peak due to the asymmetry of the VDOS of graphite or amorphous carbons towards lower wave numbers" (Ferrari and Robertson, 2000, and references therein).

Ferrari and Robertson add that "it is not always clear if the I(D)/I(G) ratio should be the ratio of the peak heights or peak areas. Generally, groups using BWF+Lorentzian fits report peak height ratios, while groups using two Gaussians report the area ratio. The difference is not so important for disordered graphite, as the peak widths are similar, but this is not so for amorphous carbons. In that case, - Ferrari and Robertson explain - the broadening of the D peak is correlated to a distribution of clusters with different orders and dimensions, and thus the information about the less distorted aromatic rings is in the intensity maximum and not in the width, which depends on the disorder. Ring orders other that six tend to decrease the peak height and increase its width" (Ferrari and Robertson, 2000). I(D)/I(G) as the ratio of peak heights is mainly used by Ferrari and Robertson in their three-stage model, by means of which we can see how the position of the G peak changes and the D peak appears.

Besides the Gaussian, Lorentzian, and BWF functions mentioned above, Voigt, pseudo-Voigt and split-Lorentzian functions are used too. And we also have q-Gaussians and split-q-Gaussians for fitting Raman spectra.

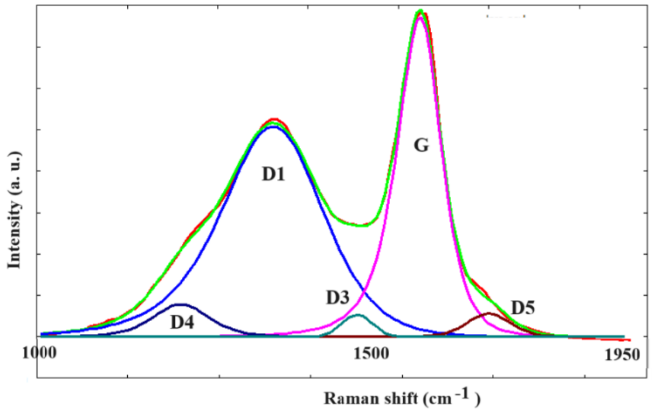

Fig. 12: As in the Figure 4, recovering the data (for biochar) from the Figure 2 by Sousa et al., 2020, we can propose a decomposition obtained by means of two split-q-Gaussian Tsallis functions for G and D1, and three q-Gaussians for D3, D4, and D5.

Lorentzian, Gaussian and q-Gaussian lineshapes

Let us return to the graphene oxides. King et al. use Lorentzian lineshape. It seems that Sardinha et al. use Lorentzian and Gaussian functions as line shapes. In both cases, areas, and positions of the peaks of Raman spectra decompositions are depending on the considered line shapes. To show that the decomposition changes according to used functions, let us the consider the data from Sardinha, given in the Fig.10, and the Fityk software (Wojdyr, 2010). Fityk is a curve fitting and data analysis application, free and open source. It can perform a Levenberg-Marquardt algorithm, among other best fit algorithms. The function of merit is the weighted sum of squared residuals (WSSR), also called chi square. Fityk has several built-in functions but allows to execute a script with user-defined functions(see in the Appendix how we can define in Fityk q-Gaussian and split-q-Gaussian functions).

Let us consider the data of GO with degree 2, from Sardinha, 2019. The best fit with Lorentzian and Gaussian functions obtained by Fityk, is given in the Figure 13; the red dots are the data, the green curve the best fit, and the blue and magenta curves the components of decomposition.

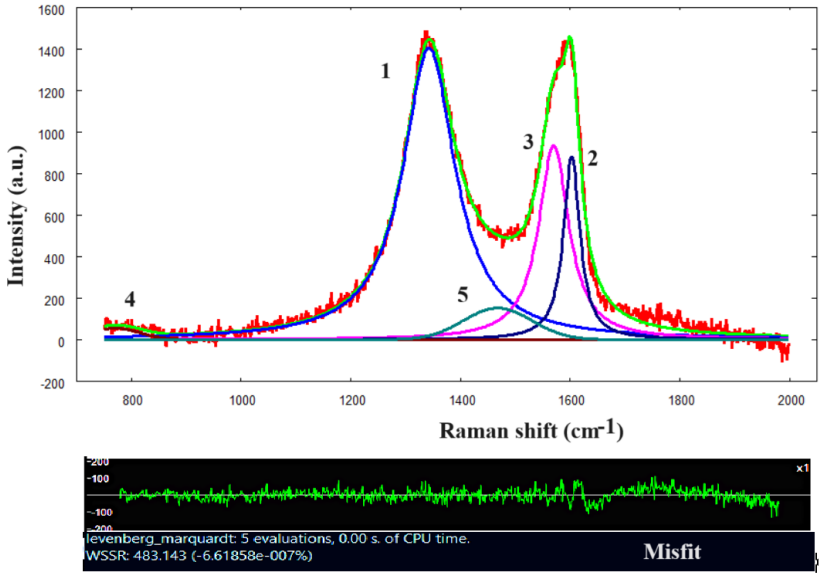

Fig.13: Curves 1,2 and 3 are Lorentzians, 4 and 5 Gaussians. Centers are 772 (5), 1343 (1, that is D1, D), 1469 (5, that is D3, D'' in Claramunt et al. notation), 1570 (3, G), and 1603 (2, D2, D'), in cm^{-1}. The lower part of the figure is giving the misfit. The sample GO2 data are a courtesy by Sardinha, 2019.

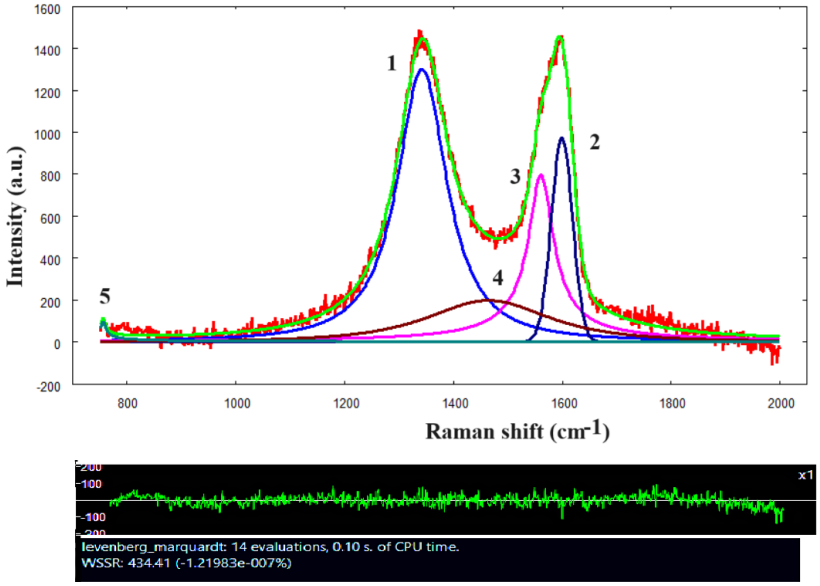

Fig.14: Curves 1-5 are q-Gaussians. Centers are 756 (5), 1342 (1, that is D1, D, q=1.89), 1465 (4, that isD3, D'' in Claramunt et al. notation, q=1.67), 1561 (3, G, q=2.43), and 1599 (2, D2, D', q=1.0), in cm^{-1}. The lower part of the figure is giving the misfit. The sample GO2 data are a courtesy by Sardinha, 2019.

In the Figure 14, a deconvolution with q-Gaussians is given. However, as suggested by Ferrari and Robertson about G peaks fitted BWF asymmetrically, we could use a split-q-Gaussian for G and a q-Gaussian for D. The result is shown in the following Figure 15.

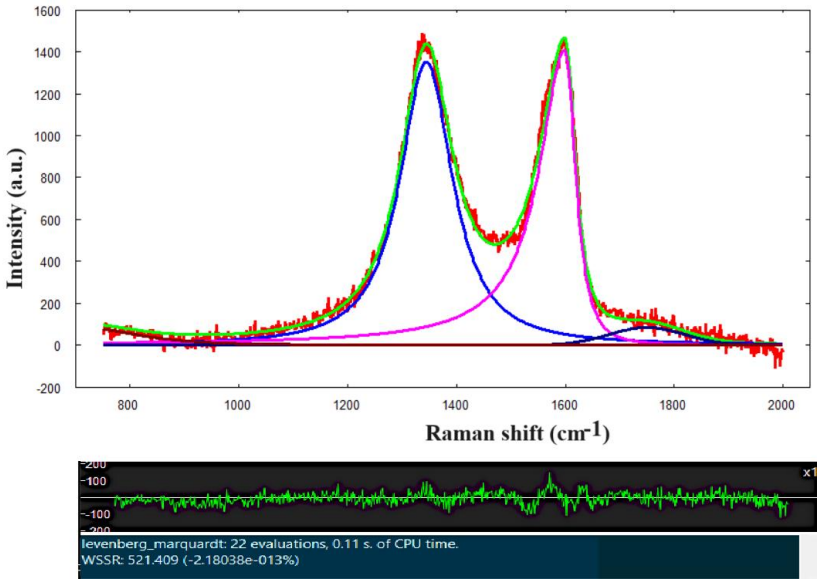

Fig.15: Data are the same as in Figs. 13 and 14. A split-q-Gaussians has been used for G peak, center 1599 cm^{-1}. For D, we used a q-Gaussian, q=1.88, center 1344 cm−1. Two further q-Gaussians have been used on the left and on the right. The sample GO2 data are a courtesy by Sardinha, 2019.

Let us pass to GO with degree 3, for instance. We can easily repeat what we did for GO with degree 2, as in the Fig. 13 and 14. However, we prefer to show the decomposition as in the Figure 15, with a slit-q-Gaussian for G, and q-Gaussian for D.

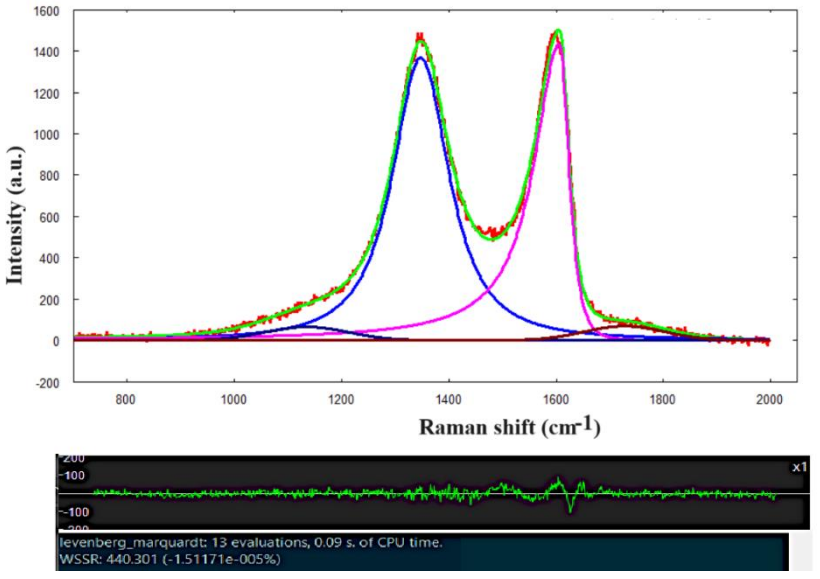

Fig.16: A split-q-Gaussians has been used for G peak, center 1605 cm−1. For D, we used a q-Gaussian, q=1.80, center 1347 cm−1. Two further q-Gaussians have been used on the left and on the right. The sample GO3 data are a courtesy by Sardinha, 2019.

As shown by the previous figures, the use of q-Gaussians instead of Lorentzian and Gaussian functions slightly

changes positions and areas of the peaks. What is deserving further consideration is the use of asymmetric split-q-Gaussian functions. We can see from Fig.15 and 16, that we do not need the D3 component.

Discussion

The analysis of all the samples proposed by Sardinha et al. is beyond the aim of this review.

Ferrari and Robertson noted that, for comparing *different fitting parameters* of the Raman spectrum, it is fundamental the knowledge of *the used fitting procedures*. Once we have decided the number of components and their line shapes, we can compare the parameters obtained from a set of Raman measurements, such as those proposed by Sardinha et al., 2020. Since *there is no a priori reason to choose a particular function to fit the spectrum*, the use of q-Gaussians is good too. As shown by several analyses of Raman spectra with q-Gaussians (see Sparavigna, 2023, 2024), these functions can be efficiently used due to the power-law of their tails. The q-Gaussian tails have an intermediate behavior, between Lorentzian and Gaussian tails, and Gaussian and Lorentzian tails are rarely observed.

For what is regarding the role of the instrumental set-up, that is of its transfer function, this function had to be deconvoluted from the recorded spectra (Rautian, 1958, Seshadri and Jones, 1963, Merlen et al., 2017). The true spectral distribution, which is subjected to "distortions both in the optical and recording parts of the apparatus" (Rautian, 1958), is replaced by the observed measured distribution. This is a further reason to stress once more that there is no a priori reason to choose a particular function to fit the spectrum, especially if we have not determined the instrumental transfer function.

Appendix – q-Gaussian and split-q-GaussianTsallis functions

The q-Gaussian functions are probability distributions proper of the Tsallis statistics (Tsallis, 1988, Hanel et al., 2009). These functions are based on a generalized form of the exponential function, characterized by a continuous real parameter q. When q is going to 1, the q-exponential becomes the usual exponential function. The value q=2, (Naudts, 2009), corresponds to the Cauchy distribution, also known as the Lorentzian distribution; the q-Gaussian function is therefore a generalization of the Lorentzian distribution too. The change of q-parameter is allowing the q-Gaussian function to pass from the Gaussian to the Lorentzian distribution.

As given by Umarov et al., 2008, the q-Gaussian function is: $f(x) = Ce_q(-\beta x^2)$, where $e_q(.)$ is the q-exponential function and C a scale constant (in the exponent, $\beta = 1/(2\sigma^2)$). The q-exponential has expression: $e_q(u) = [1 + (1-q)u]^{1/(1-q)}$. The plots in the Figures A.1 and A.2 are showing the behaviour of this exponential for different q values. Note that, for q less than one, the function is different from zero on a limited interval.

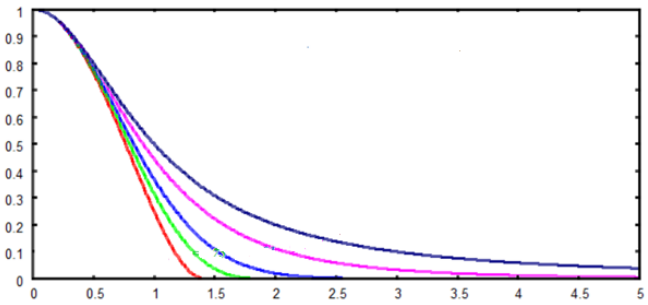

Fig.A.1: q- exponential functions, where the blue curve is representing a Lorentzian function (q=2). The pink curve corresponds to q=1.5 and light blue to q= 1.01, practically a Gaussian function. The green curve is the q-Gaussian for q=0.75 and red curve for q=0.5. For q < 1, the function is different from zero in a limited interval. Being the line symmetric, only the right side of it is given in the figure.

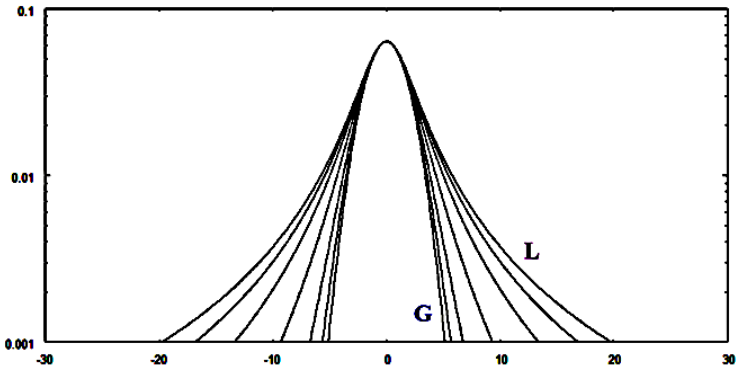

Fig.A.2: q-Gaussians, between the Lorentzian L and the Gaussian G function, in a log scale for the y-axis (semi log scale).

The Half Width at Half Maximum of q line shape is given by: $\sqrt{2}\sigma\sqrt{(1-(1/2)|1-q)/(1-q)}$.
To have an asymmetric form of the q-Gaussian function, let us write it in the following manner (the center of the band is at x_o):

$$\text{q-Gaussian} = Cexp_q(-\beta(x-x_o)^2) = C[1-(1-q)\beta(x-x_o)^2]^{1/(1-q)}$$

In ChemRxiv we considered the asymmetric q-Gaussians, as given by Devi (2021):

$$\text{q-Gaussian}_{\text{LEFT}} = Cexp_{q_L}(-\beta_L(x-x_o)^2) = C[1-(1-q_L)\beta_L(x-x_o)^2]^{1/(1-q_L)}, \text{ when } x-x_o<0$$

$$\text{q-Gaussian}_{\text{RIGHT}} = Cexp_{q_R}(-\beta_R(x-x_o)^2) = C[1-(1-q_R)\beta_R(x-x_o)^2]^{1/(1-q_R)}, \text{ when } x-x_o>0$$

Parameters q and β of the Left and the Right parts are different. The most proper name for this asymmetric function is split-q-Gaussian. We could also generalized the Breit-Wigner-Fano into a q-Breit-Wigner-Fano.
In Fityk, a q-Gaussian function can be defined in the following manner:

define Qgau(height, center, hwhm, q=1.5) = height*(1+(q-1)*((x-center)/hwhm)^2)^(1/(1-q))

q=1.5 the initial guessed value of the q-parameter. Parameter hwhm is the half width at half maximum of the component. When q=2, the q-Gaussian is a Lorentzian function, that we can find defined in Fityk as:

Lorentzian(height, center, hwhm) = height/(1+((x-center)/hwhm)^2)

When q is close to 1, the q-Gaussian becomes a Gaussian function. The split q-Gaussian is defined as:

Splitqgau(height, center, hwhm1=hwhm, hwhm2=hwhm, q1=1.5, q2=1.5) = x < center ? Qgau(height, center, hwhm1, q1) : Qgau(height, center, hwhm2, q2)

The split Lorentzian is: SplitLorentzian(height, center, hwhm1=hwhm, hwhm2=hwhm) = x < center ? Lorentzian(height, center, hwhm1) : Lorentzian(height, center, hwhm2)

References

1. Basko, D. M., Piscanec, S., & Ferrari, A. C. (2009). Electron-electron interactions and doping dependence of the two-phonon Raman intensity in graphene. Physical Review B, 80(16), 165413.

2. Beyssac, O., Goffé, B., Chopin, C., & Rouzaud, J. N. (2002). Raman spectra of carbonaceous material in metasediments: a new geothermometer. Journal of metamorphic Geology, 20(9), 859-871.
3. Brodie, B. C. (1860). Sur le poids atomique du graphite. Ann. Chim. Phys, 59(466), e472.
4. Childres, I., Jauregui, L. A., Park, W., Cao, H., & Chen, Y. P. (2013). Raman spectroscopy of graphene and related materials. New developments in photon and materials research, 1, 1-20.
5. Claramunt, S., Varea, A., Lopez-Diaz, D., Velázquez, M. M., Cornet, A., & Cirera, A. (2015). The importance of interbands on the interpretation of the Raman spectrum of graphene oxide. The Journal of Physical Chemistry C, 119(18), 10123- 10129.
6. Cui, L., & Sun, M. (2021). Graphene plasmon-enhanced polarization-dependent interfacial charge transfer excitons in 2D graphene-black phosphorus heterostructures in NIR and MIR regions. The Journal of Physical Chemistry C, 125(40), 22370-22378.
7. Devi, S. (2021). Asymmetric Tsallis distributions for modeling financial market dynamics. Physica A: Statistical Mechanics and Its Applications, 578, 126109
8. Dikin, D. A., Stankovich, S., Zimney, E. J., Piner, R. D., Dommett, G. H., Evmenenko, G., Nguyen, S. T., & Ruoff, R. S. (2007). Preparation and characterization of graphene oxide paper. Nature, 448(7152), pp.457-460.
9. Ejehi, F., Mohammadpour, R., Asadian, E., Sasanpour, P., Fardindoost, S., & Akhavan, O. (2020). Graphene oxide papers in nanogenerators for self-powered humidity sensing by finger tapping. Scientific reports, 10(1), 7312.
10. Fenske, M. R., Braun, W. G., Wiegand, R. V., Quiggle, D., McCormick, R., & Rank, D. H. (1947). Raman spectra of hydrocarbons. Analytical Chemistry, 19(10), 700-765.
11. Ferrari, A. C. (2007). Raman spectroscopy of graphene and graphite: Disorder, electron–phonon coupling, doping and nonadiabatic effects. Solid state communications, 143(1-2), 47-57.
12. Ferrari, A. C., & Basko, D. M. (2013). Raman spectroscopy as a versatile tool for studying the properties of graphene. Nature nanotechnology, 8(4), 235-246.
13. Ferrari, A. C., Meyer, J. C., Scardaci, V., Casiraghi, C., Lazzeri, M., Mauri, F., Piscanec, S., Jiang, D., Novoselov, K. S., Roth, S., & Geim, A. K. (2006). Raman spectrum of graphene and graphene layers. Physical Review Letters 97: 187401.
14. Ferrari, A. C., & Robertson, J. (2000). Interpretation of Raman spectra of disordered and amorphous carbon. Physical Review B 61: 14095–14107.
15. Frisenda, R., Niu, Y., Gant, P., Muñoz, M., & Castellanos-Gomez, A. (2020). Naturally occurring van der Waals materials. npj 2D Materials and Applications, 4(1), 38.
16. Gavilan, L., Ricketts, C. L., Bejaoui, S., Ricca, A., Boersma, C., Salama, F., & Mattioda, A. L. (2022). Raman spectroscopic study of pyrene in cosmic dust analogues: evolution from the gas to the solid phase. ACS Earth and Space Chemistry, 6(9), 2215-2225.
17. Geim, A. K., & Novoselov, K. S. (2007). The rise of graphene. Nature materials, 6(3), 183-191.
18. Goldie, S. J., Bush, S., Cumming, J. A., & Coleman, K. S. (2020). A statistical approach to Raman analysis of graphene-related materials: implications for quality control. ACS Applied Nano Materials, 3(11), 11229-11239.
19. Gupta, A., Chen, G., Joshi, P., Tadigadapa, S., & Eklund. (2006). Raman scattering from high-frequency phonons in supported n-graphene layer films. Nano letters, 6(12), 2667-2673.
20. Haidari, M. M., Kim, H., Kim, J. H., Park, M., Lee, H., & Choi, J. S. (2020). Doping effect in graphene-graphene oxide interlayer. Scientific Reports, 10(1), 8258.
21. Hanel, R., Thurner, S., & Tsallis, C. (2009). Limit distributions of scale-invariant probabilistic models of correlated random variables with the q-Gaussian as an explicit example. The European Physical Journal B, 72(2), 263.

22. Hummers, W., & Offeman, R. (1958). Preparation of graphitic oxide. J. Am. Chem. Soc. 80, 1339.

23. Jorio, A., Dresselhaus, M., Saito, R., & Dresselhaus, G. F. (2011). RamanSpectroscopy in Graphene Related Systems; WILEY-VCH Verlag GmbH& Co. KGaA: Weinheim, Germany

24. King, A. A. K., Davies, B. R., Noorbehesht, N., Newman, P., Church, T.L., Harris, A. T., Razal, J. M., & Minett, A. I. (2016). A new Raman metric for the characterisation of graphene oxide and its derivatives. Scientific Reports 6(1),1–6, http://dx.doi.org/10.1038/srep19491.

25. Knight, D. S., & White, W. B. (1989). Characterization of diamond films by Raman spectroscopy. Journal of Materials Research, 4, 385-393.

26. Krishnan, R. S. (1945). Raman spectrum of diamond. Nature, 155(3928), 171-171.

27. Lerf, A., He, H., Forster, M., & Klinowski, J. (1998). Structure of Graphite Oxide Revisited. J. Phys. Chem. B,102, 4477−4482

28. Li, Z., Deng, L., Kinloch, I. A., & Young, R. J. (2023). Raman spectroscopy of carbon materials and their composites: Graphene, nanotubes and fibres. Progress in Materials Science, 135, 101089.

29. Lin-Vien, D., Colthup, N. B., Fateley, W. G., & Grasselli, J. G. (1991). The handbook of infrared and Raman characteristic frequencies of organic molecules. Elsevier.

30. Liu, Y. H., Ma, Z. K., He, Y., Wang, Y., Zhang, X. W., Song, H. H., & Li, C. X. (2023). A review of fibrous graphite materials: graphite whiskers, columnar carbons with a cone-shaped top, and needle-and rods-like polyhedral crystals. New Carbon Materials, 38(1), 18-35.

31. Lucchese, M.M., Stavale, F., Ferreira, E.M., Vilani, C., Moutinho, M.V.D.O., Capaz, R.B., Achete, C.A., & Jorio, A. (2010). Quantifying ion-induced defects and Raman relaxation length in graphene. Carbon, 48(5), pp.1592-1597.

32. Malard, L. M., Pimenta, M. A., Dresselhaus, G., & Dresselhaus, M. S. (2009). Raman spectroscopy in graphene. Physics reports, 473(5-6), 51-87.

33. Mapelli, C. (1998). Tesi di Laurea, Politecnico di Milano.

34. Mapelli, C., Castiglioni, C., Zerbi, G., & Müllen, K. (1999). Common force field for graphite and polycyclic aromatic hydrocarbons. Physical Review B, 60(18), 12710.

35. Merlen, A., Buijnsters, J. G., & Pardanaud, C. (2017). A guide to and review of the use of multiwavelength Raman spectroscopy for characterizing defective aromatic carbon solids: Fromgraphene to amorphous carbons. Coatings, 7(10), 153.

36. Milani, A., Tommasini, M., Russo, V., Bassi, A. L., Lucotti, A., Cataldo, F., & Casari, C. S. (2015). Raman spectroscopy as a tool to investigate the structure and electronic properties of carbon-atom wires. Beilstein journal of nanotechnology, 6(1), 480-491.

37. Mishra A.K., & Ramaprabhu S. (201). Hybrid carbon nanostructure assemblage for high performance pseudo-capacitors. AIP Adv. 2, http://dx.doi.org/10.1063/1.4717490.

38. Mu, X., & Sun, M. (2020). The linear and non-linear optical absorption and asymmetrical electromagnetic interaction in chiral twisted bilayer graphene with hybrid edges. Materials Today Physics, 14, 100222. 10.1016/j.mtphys.2020.100222.

39. Naudts, J. (2009). The q-exponential family in statistical physics. Central European Journal of Physics, 7, 405-413.

40. Nemanich, R. J., Solin, S. A., & Martin, R. M. (1981). Light scattering study of boron nitride microcrystals. Physical Review B, 23(12), 6348.

41. Novoselov, K.S., Geim, A.K., Morozov, S.V., Jiang, D.E., Zhang, Y., Dubonos, S.V., Grigorieva, I.V., & Firsov, A.A. (2004). Electric field effect in atomically thin carbon films. science, 306(5696), pp.666-669.

42. O'Brien, C. (2023). Graphene Market & 2D Materials Assessment 2024-2034: Technologies, Markets, Players.

IDTechEx ISBN 9781915514967

43. Ott, A. K., & Ferrari, A. C. (2024). Raman spectroscopy of graphene and related materials. Encyclopedia of Condensed Matter Physics, 2nd ed.; Chakraborty, T., Ed, 233-247.
44. Rautian, S. G. (1958). Real spectral apparatus. Soviet Physics Uspekhi, 1(2), 245
45. Sadezky, A., Muckenhuber, H., Grothe, H., Niessner, R., & Pöschl, U. (2005). Raman microspectroscopy of soot and related carbonaceous materials: Spectral analysis and structural information. Carbon, 43(8), 1731-1742.
46. Saito, R., Hofmann, M., Dresselhaus, G., Jorio, A., & Dresselhaus, M. S. (2011). Raman spectroscopy of graphene and carbon nanotubes. Advances in Physics, 60(3), 413-550.
47. Sardinha, A. (2019). Raman spectra of Graphene oxide, Mendeley Data, V1, doi: 10.17632/n4nts7hvvx.1
48. Sardinha, A. (2019), Raman spectra of Graphene oxide, Mendeley Data, V2, doi: 10.17632/n4nts7hvvx.2
49. Sardinha, A. F., Almeida, D. A., & Ferreira, N. G. (2020). Electrochemical impedance spectroscopy correlation among graphene oxide/carbon fibers (GO/CF) composites and GO structural parameters produced at different oxidation degrees. Journal of Materials Research and Technology, 9(5), 10841-10853.
50. Schniepp, H.C., Li, J.L., McAllister, M.J., Sai, H., Herrera-Alonso, M., Adamson, D.H., Prud'homme, R.K., Car, R., Saville, D.A., & Aksay, I.A. (2006). Functionalized single graphene sheets derived from splitting graphite oxide. The journal of physical chemistry B, 110(17), pp.8535-8539.
51. Seshadri, K., & Jones, R. N. (1963). The shapes and intensities of infrared absorption bands—A review. Spectrochimica Acta, 19(6), 1013-1085
52. Shuker, R., & Gammon, R. W. (1970). Raman-scattering selection-rule breaking and the density of states in amorphous materials. Physical Review Letters, 25(4), 222.
53. Siklitskaya, A., Gacka, E., Larowska, D., Mazurkiewicz-Pawlicka, M., Malolepszy, A., Stobiński, L., Marciniak, B., Lewandowska-Andrałojć, A., & Kubas, A. (2021). Lerf–Klinowski-type models of graphene oxide and reduced graphene oxide are robust in analyzing non-covalent functionalization with porphyrins. Scientific reports, 11(1), p.7977.
54. Sousa, D. V. D., Guimarães, L. M., Felix, J. F., Ker, J. C., Schaefer, C. E. R., & Rodet, M. J. (2020). Dynamic of the structural alteration of biochar in ancient Anthrosol over a long timescale by Raman spectroscopy. PloS one, 15(3), e0229447.
55. Sparavigna, A. C. (2023). q-Gaussian Tsallis Line Shapes and Raman Spectral Bands. Int. J. Sciences, 12(3), 27-40, 2023, http://dx.doi.org/10.18483/ijSci.2671 Available at SSRN: https://ssrn.com/abstract=4398623
56. Sparavigna, A. C. (2023). q-Gaussian Tsallis Line Shapes for Raman Spectroscopy (June 7, 2023). SSRN Electronic Journal. http://dx.doi.org/10.2139/ssrn.4445044
57. Sparavigna, A. C. (2023). SERS Spectral Bands of L-Cysteine, Cysteamine and Homocysteine Fitted by Tsallis q-Gaussian Functions. International Journal of Sciences, 12(09), 14–24. https://doi.org/10.18483/ijsci.2721
58. Sparavigna, A. C. (2024). Raman Spectroscopy of Siderite with q-Gaussian and split-q-Gaussian Analyses. International Journal of Sciences, 13(02), 8-21.
59. Sparavigna, A. C. (2024). Pyrene and Biochar (Raman Spectroscopy). ChemRxiv. doi:10.26434/chemrxiv-2024-7zbtf
60. Stankovich, S., Dikin, D.A., Piner, R.D., Kohlhaas, K.A., Kleinhammes, A., Jia, Y., Wu, Y., Nguyen, S.T., & Ruoff, R.S. (2007). Synthesis of graphene-based nanosheets via chemical reduction of exfoliated graphite oxide. carbon, 45(7), pp.1558-1565.
61. Stankovich, S., Piner, R.D., Chen, X., Wu, N., Nguyen, S.T., & Ruoff, R.S. (2006). Stable aqueous dispersions of graphitic nanoplatelets via the reduction of exfoliated graphite oxide in the presence of poly (sodium 4-styrenesulfonate). Journal of Materials Chemistry, 16(2), pp.155-158.
62. Stankovich, S., Piner, R.D., Nguyen, S.T., & Ruoff, R.S. (2006). Synthesis and exfoliation of isocyanate-treated

graphene oxide nanoplatelets. Carbon, 44(15):3342–7.

63. Stankovich, S., Dikin, D.A., Dommett, G.H., Kohlhaas, K.M., Zimney, E.J., Stach, E.A., Piner, R.D., Nguyen, S.T. , & Ruoff, R.S. (2006). Graphene-based composite materials. nature, 442(7100), pp.282-286.
64. Staudenmaier, L. (1898). Verfahren zur darstellung der graphitsäure. Berichte der deutschen chemischen Gesellschaft, 31(2), 1481-1487.
65. Staudenmaier, L. (1899). Verfahren zur darstellung der graphitsäure. Berichte der deutschen chemischen Gesellschaft, 32(2), 1394-1399.
66. Tan, P., Hu, C., Dong, J., Shen, W., & Zhang, B. (2001). Polarization properties, high-order Raman spectra, and frequency asymmetry between Stokes and anti-Stokes scattering of Raman modes in a graphite whisker. Physical Review B, 64(21), 214301.
67. Thomsen, C., & Reich, S. (2000) Double resonant Raman scattering in graphite. Physical Review Letters 85: 5214–5217.
68. Tsallis, C. (1988). Possible generalization of Boltzmann-Gibbs statistics. Journal of statistical physics, 52, 479-487.
69. Tuinstra, F., & Koenig, J. L. (1970) Raman spectrum of graphite. The Journal of Chemical Physics 53, 1126–1130.
70. Umarov, S., Tsallis, C., Steinberg, S. (2008). On a q-Central Limit Theorem Consistent with Nonextensive Statistical Mechanics. Milan J. Math. Birkhauser Verlag. 76: 307–328. doi:10.1007/s00032-008-0087-y. S2CID 55967725.
71. Wojdyr, M. (2010). Fityk: a general-purpose peak fitting program. Journal of Applied Crystallography, 43(5-1), 1126-1128.
72. Wu, J. B., Lin, M. L., Cong, X., Liu, H. N., & Tan, P. H. (2018). Raman spectroscopy of graphene-based materials and its applications in related devices. Chemical Society Reviews, 47(5), 1822-1873.
73. Zhang, C. C., Hartlaub, S., Petrovic, I., & Yilmaz, B. (2022). Raman spectroscopy characterization of amorphous coke generated in industrial processes. ACS omega, 7(3), 2565-2570.